minerals

MDPI

Article

# Solubility Product of Vanadinite $Pb_5(VO_4)_3Cl$ at 25 °C—A Comprehensive Approach to Incongruent Dissolution Modeling

**Justyna Topolska [1,*], Bartosz Puzio [1], Olaf Borkiewicz [2], Julia Sordyl [1] and Maciej Manecki [1]**

[1] Department of Mineralogy, Petrography and Geochemistry, Faculty of Geology, Geophysics and Environmental Protection, AGH University of Science and Technology, al. Mickiewicza 30, 30-059 Kraków, Poland; bpuzio@agh.edu.pl (B.P.); sordyljulia@gmail.com (J.S.); gpmmanec@cyf-kr.edu.pl (M.M.)

[2] X-ray Science Division, Advanced Photon Source, Argonne National Laboratory, 9700 South Cass Avenue, Bldg. 433, Argonne, IL 60439-4858, USA; borkiewicz@aps.anl.gov

* Correspondence: topolska@agh.edu.pl

**Abstract:** Although vanadinite ($Pb_5(VO_4)_3Cl$) occurs in abundance in various terrestrial geochemical systems of natural and anthropogenic origin and is seriously considered as a potential nuclear waste sequestering agent, its actual application is severely limited by a lack of understanding of its basic thermodynamic parameters. In this regard, the greatest challenge is posed by its incongruent dissolution, which is a pivotal hurdle for effective geochemical modeling. Our paper presents an universal approach for geochemical computing of systems undergoing incongruent dissolution which, along with unique, long-term experiments on vanadinites' stability, allowed us to determine the mineral solubility constant. The dissolution experiments were carried out at pH = 3.5 for 12 years. Vanadinite has dissolved incongruently, continuously re-precipitating into chervetite ($Pb_2V_2O_7$) with the two minerals remaining in mutual equilibrium until termination of the experiments. The empirically derived solubility constant $K_{sp,V,298} = 10^{-91.89 \pm 0.05}$ of vanadinite was determined for the first time. The proposed modeling method is versatile and can be adopted to other mineral systems undergoing incongruent dissolution.

**Keywords:** lead apatite; chervetite; solubility product; dissolution experiment; thermodynamics; geochemical modeling

check for updates

**Citation:** Topolska, J.; Puzio, B.; Borkiewicz, O.; Sordyl, J.; Manecki, M. Solubility Product of Vanadinite $Pb_5(VO_4)_3Cl$ at 25 °C—A Comprehensive Approach to Incongruent Dissolution Modeling. *Minerals* **2021**, *11*, 135. https://doi.org/10.3390/min11020135

Academic Editor: Felix Brandt
Received: 9 January 2021
Accepted: 25 January 2021
Published: 29 January 2021



## 1. Introduction

Vanadium is one of the most important metals in modern technology. It is the twenty-second most common element in the Earth's crust and the fifth most common transition metal. Small amounts of vanadium are essential for metabolism of several bacteria, algae, fungi and lichens (e.g., [1–5]). It also partakes in several bodily functions and life processes [6]. Vanadinite $Pb_5(VO_4)_3Cl$ is a secondary mineral, usually found in the oxidation zones of lead deposits and as a product of corrosion of infrastructure. In nature, it is often associated with high V content in mica and clay sediments subjected to hydrothermal processes, occurring under neutral or slightly alkaline conditions [7–9]. However, the mineral was also found in lead pipe water systems and it occurs in many already closed lead mines around the world [10,11]. Overall, there are more than 3000 worldwide locations, where vanadinite is present along with its phosphate and arsenate counterparts: pyromorphite $Pb_5(PO_4)_3Cl$ and mimetite $Pb_5(AsO_4)_3Cl$ [12], with which it forms solid solution series [13–15]. The minerals belong to the group of lead apatites [16], the composition of which is expressed by the general formula $Pb_5(BO_4)_3X$, where $BO_4$ represents the coordinated tetrahedron oxyanions (e.g., $PO_4^{3-}$, $AsO_4^{3-}$, $VO_4^{3-}$) and $X$ represents the monovalent electronegative anions (e.g., $F^-$, $Cl^-$, $Br^-$, $I^-$, $OH^-$) [17–19]. The hexagonal structure of most of the minerals in this group is consistent with the apatite structure

$Ca_5(PO_4)_3F$ (spatial group P63/m) [14,17,19–24]. Many mineral phases of the apatite group are promising in the stabilization and recycling of industrial and nuclear waste and are being intensively studied in this respect [25–35]. The lead apatites are particularly interesting in this matter due to their relatively low solubility products, e.g., [36–39]. For this reason, induced precipitation of pyromorphite ($\log K_{sp} \sim -79$) by phosphates amendments to soil or waste is a proposed and applied method of in situ remediation of lead-contaminated sites ([40–43] and the literature cited therein). Pentavalent vanadium in the form of $VO_4^{3-}$ anion, one of the building blocks of vanadinite, is the most toxic and mobile form of the element that bears the potential of having a major impact on human health in the near future [44,45]. Furthermore, the level of vanadium in the environment is increasing alarmingly and its spread due to the combustion of hydrocarbon fuels, industrial and mining activities has been of concern in recent decades [46,47]. Therefore, the increasing number of studies on vanadinites as sequestering agents is not surprising [26,48–51]. However, the stability of vanadinites is, to date, poorly understood [10,52] and both the missing solubility and thermodynamic data are of high importance for a wide range of remediation strategies geared towards reducing the effects of potentially toxic substances containing Pb, V, As and radioactive elements [27]. Determination of the solubility product of vanadinite ($K_{sp,V}$) poses significant challenges and, to date, no reliable data on this matter have been presented. Gerke et al. [10] in their studies of groundwater in the Pb-containing pipes, proposed a $\log K_{sp,V}$ value of –86, but their approach to estimate the solubility of vanadinite failed to consider fundamentals of thermodynamic modeling regarding congruency of dissolution and solution equilibrium. As such, the authors themselves recommended continued investigations into the matter. Unlike orthophosphate or orthoarsenate ions, orthovanadate groups tend to polymerize in aqueous solution (e.g., [53]). Hence, the difficulty in determining $K_{sp,V}$ stems from the fact that it is prone to re-precipitation into its polymerized form—chervetite ($Pb_2(V_2O_7)$)—under a wide range of conditions [54]. During the incongruent dissolution of vanadinite—as the system approaches thermodynamic equilibrium, a key factor in determining the properties of the minerals—chervetite is formed. Recrystallization is relatively slow and occurs at different rates, which highly depend on the pH and temperature; however, this process is still poorly understood in the context of vanadinite solubility [55]. In the carbonaceous environments, the amount of adsorbed (or possibly precipitated as chervetite) vanadium is greatly affected by the dissolved organic compounds (humic substances, organic acids) because of reduction of vanadate V(V) to vanadyl (V(IV)) $VO^{2+}$ ions [56–59]. Furthermore, thermodynamic modelling of incongruent dissolutions poses significant challenges and, even though it is relevant to a large number of mineralogical systems, including other apatites, few approaches have been proposed to date, and no universal method can be referenced [60–63].

The growing importance of lead vanadate phases for industrial and environmental applications, along with the obvious lack of reliable thermodynamic data for vanadinite as the endmember of Pb-apatites solid solutions series, has served as an inspiration for the presented unconventional, 12-year long experiment on its solubility and stability. Our aim was to supplement thermodynamic data and to provide a reliable basis for further studies on Pb-V phases. We have faced the challenge of incongruent dissolution and, in this work, we demonstrate an approach to data processing that allowed us to experimentally determine the solubility product of vanadinite for the first time, and which is also sufficiently universal to be applied to other systems.

## 2. Materials and Methods

### *2.1. Synthesis of Vanadinite*

Synthesis of vanadinite was carried out at 90 °C and pH 3.5 adjusted using 0.1 M $HNO_3$ (MERCK, supra pure) by dropwise mixing of the aqueous solutions of $Pb(NO_3)_2$ (POCH.SA, pure for analysis), KCl (CHEMPUR, pure for analysis), and $NH_4VO_3$ (POCH.SA, pure for analysis), in molar proportions based on the stoichiometry of the vanadinite (Pb:V:Cl = 5:3:1 molar ratio). The temperature and the pH of the synthesis were indicated by preliminary

geochemical modeling [64,65] as the conditions favorable for the $VO_4^{3-}$ presence in the solution, thus favorable for vanadinite precipitation. Suspension of forming precipitate was stirred using a mechanical stirrer for 5 h and then allowed to settle. After 2 weeks, the precipitate was separated from the solutions by decantation, washed thoroughly several times with redistilled water and acetone and dried at 110 °C.

### 2.2. Solid Characterization

The X-ray powder diffraction (XRD) pattern of the solids was obtained using a Philips PW 3020 X'Pert-APD Diffractometer system (with a Cu anode and a graphite monochromator) using a step scan mode at a step size of 0.02° 2Θ and a rate of 1 s per step. The scanning electron microscopy with elemental microanalysis (SEM/EDS) was performed using a variable pressure field emission FEI QUANTA 200 FEG microscope on gold-coated and uncoated samples at 20 kV. For the wet chemical analysis, -small portions of synthetic vanadinite (~50 mg) were digested in 0.02 M EDTA (2,2′,2′′,2′′′—(ethane−1,2-diyldinitrilo)tetraacetic acid) (POCH.SA, pure for analysis) and analyzed for Pb, V and Cl, as described in the next section. Compared to other reagents e.g., $HNO_3$, the EDTA is an effective solvent for mineralization of Pb-apatites yielding relatively quick and complete dissolution of the solid [14,36,37,39,55].

### 2.3. Solution Analysis

A Total Reflection X-ray Fluorescence was used to determine the Pb and V content in the solutions resulting from dissolution experiments. The samples were inoculated with a nickel stock solution (1000 mg $dm^{-3}$, MERCK, supra pure) as an internal standard, and analyzed at 50 kV and 12 mA with a Nanohunter II spectrometer equipped with a Mo lamp (t = 3000 s). Atomic Absorption Spectroscopy AAS (SavantAA GBC Scientific Equipment) was used to determine the concentration of Pb and V in the solutions resulting from digestion of solids in EDTA for wet chemical analysis of vanadinite. The turbidimetric method, with silver nitrate at 380 nm, was used to determine the concentration of Cl in all solutions with a HITACHI U-1800 UV-Vis Spectrophotometer. The universal meter CX-505 with a glass pH electrode ERH-13-6 was used to measure the pH. All analyses were performed in triplicate.

### 2.4. Dissolution Experiments

Dissolution experiments were performed in triplicate in 250 mL polycarbonate bottles at 25 °C ± 1 °C. Equal portions (150 mg) of synthetic vanadinite were washed thoroughly with redistilled water and introduced as a suspension to the bottles containing 250 mL of 0.05 M $KNO_3$ solution. The $KNO_3$ (POCH.SA, pure for analysis) was used as the background electrolyte because both, $K^+$ and $NO_3^-$ ions are not involved in the reactions in the studied experimental system. At this concentration of the background electrolyte, the increase in ion concentration caused by the dissolution of the mineral during the experiment does not cause significant changes in the total ionic strength of the solution, and thus does not affect the experimental conditions. At the same time, the ionic strength is low enough that the Debye-Hückel equation can be used to calculate ion activity. The experiments were performed in triplicate at pH = 3.5, adjusted using 0.1 M $HNO_3$ (MERCK, supra pure). This pH value was indicated in our previous studies as adequate for the potential thermodynamic modeling of vanadinite stability [55]. The dissolution was carried out for 12 years. For the first 8 months, the bottles were immersed in a closed water bath with thermostatic control and manually stirred at least two times a week. After this time, the bottles were transferred to a room temperature of 22 °C ± 2 °C and kept for 9 years in darkness; the reactors were occasionally mixed and checked for leaks. For the last 3 years of the experiments, the temperature was raised to 25 °C ± 1 °C and the reactors were manually stirred at least once a month. During the experiments, 4 mL aliquots of the solutions were collected periodically, filtered using a 0.2 µm polycarbonate filter and analyzed in terms of pH and the total concentration of Pb, V and Cl. The evolution

pattern of [Pb], [V] and [Cl] was observed to determine the equilibrium in the suspensions; the system was considered in equilibrium when the results of three consecutive solution analyses were equal at 95% confidence level. The residual solids were syringe-sampled, washed with acetone, air-dried, and characterized with SEM/EDS and XRD.

### *2.5. Statistics*

The statistical software Statistica 13 (StatSoft Polska) was used to process the solution composition data. The normal distribution was verified with the use of the Kolmogorov–Smirnov (K–S) test with Lilliefors correction (K–S–L) and the Shapiro–Wolf test (S–W). The Wald–Wolfowitz, the U Mann–Whitney and the Kołmogorow–Smirnow tests and the Student's t test were applied accordingly to verify whether the elemental contents of the solutions change significantly over time at 95% confidence level.

## 3. Results

### *3.1. Synthesized Solid*

The synthesis yielded very fine, crystalline vanadinite with crystals smaller than 2 µm (Figure 1). Lead, vanadium, chlorine, and oxygen were the only elements detected by the SEM/EDS elemental microanalysis (data not shown). No other crystalline or amorphous components were observed. Comparison of XRD patterns with data reported by Dai and Hughes [66] and Trotter and Barnes [67] yielded good agreement, indicating vanadinite $Pb_5(VO_4)_3Cl$ as the sole reaction product (Table A1). No other phases were found within the detection limit of the method (equal to ca. 0.1 wt%). The wet chemical analysis of synthesized solid confirmed the purity of the solid (mass fraction purity = 0.995).

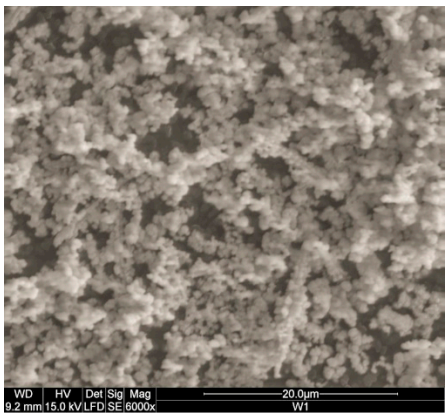


**Figure 1.** SEM microphotograph of synthetic vanadinite. The precipitate was aged for 2 weeks.

### *3.2. Dissolution Experiments*

The dissolution experiments were carried out over an exceptionally long period—12 years. Standard empirical thermodynamic studies of apatites last several weeks, as this has been widely accepted to be sufficiently long for the solids to equilibrate with the solutions [36,37,39,68]. However, vanadates tend to polymerize, inducing re-precipitation of vanadinite $Pb_5(VO_4)_3Cl$ into chervetite $Pb_2V_2O_7$; the system is highly pH and temperature dependent and the kinetics of these reactions are poorly understood [55]. This caused difficulties in the interpretation of dissolution data and in unambiguous determination of the equilibrium of the system with the use of the dissolution–precipitation method (e.g., [37]). Thus, we decided to run the experiments over an exceptionally long period, recognizing the long-term stability of the solutions' composition as the sufficient base to estimate the missing thermodynamic parameters for vanadinite. The analytical methods (TXRF), requiring small amounts of aliquots, as well as the proper sealing of the reactors assured the quality of the long-term experiments, and the effect of potential evaporation was negligible.

The SEM image of the dissolution residue after 12 years of aging in the suspension is presented in Figure 2. During the experiments, apart from the very fine, hexagonal particles of primary vanadinite, (the experimental material subject to dissolution; please compare with Figure 1), notably larger (>10 µm) prismatic crystals with the monoclinic symmetry appeared in the solid fraction. The EDS (data not shown) and the XRD analysis indicated that the prismatic crystals of the secondary mineral phase are chervetite $Pb_2V_2O_7$. [69,70]. All X-ray diffraction peaks were assigned to either vanadinite or chervetite, confirming beyond doubt the incongruent nature of the dissolution process in which vanadinite re-precipitates partially into chervetite (Table A1). The possible mechanism behind the appearance of chervetite in the solid residue was that dissolving vanadinite released Pb and V ions in concentrations exceeding the solubility product of chervetite inducing its precipitation as the secondary mineral. However, the recrystallization of vanadinite into chervetite due to adsorption of polymerized vanadates or their direct formation on the vanadinite surface cannot be excluded.

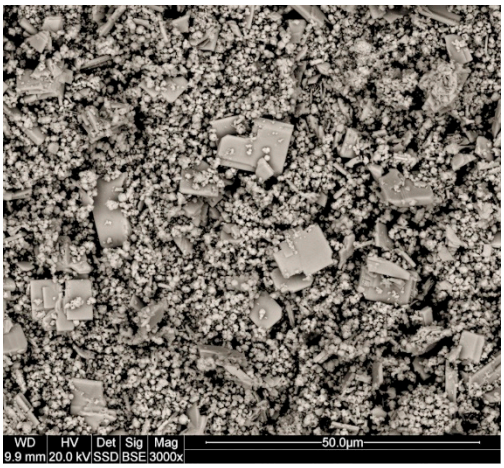


**Figure 2.** SEM microphotographs of the residual solids from the dissolution experiments of vanadinite. Fine, hexagonal, stubby crystals were identified as vanadinite while notably larger, tabular ones were identified as chervetite.

The evolution of Pb, V and Cl concentration in the experimental solutions with time is shown in Table 1 and additionally visualized in Figure A1 (Appendix B) The pH was systematically measured; however, its value remained stable for the whole 12 years, oscillating at 3.5 ± 0.05, hence the data was not included in the table. The applied statistical analysis yielded that at the 95% confidence level the solution samples collected within the 1st, 2nd, 5th, 8th and 19th week as well as the 116th, 132th and 147th month of the experiment were identical in terms of Cl concentration. This indicated that Cl had reached its close-to-equilibrium level in the solutions relatively quickly, i.e., within the first week of the experiment. In contrast, the concentrations of $Pb_{tot}$ and $V_{tot}$ systematically increased in the solutions and only the last three samples collected during the final 3 years of the experiment were statistically identical at 95% confidence level (Table 1). It is worth mentioning that vanadium concentration in most of the samples collected at the beginning of the experiment was below or at its detection limit (0.5 µmol $dm^{-3}$). The results suggested that the system had reached significant, long-term steady state conditions: three years of statistically stable solution parameters. Hence, we concluded that the final levels (in µmol $dm^{-3}$) of Cl = 24.4 ± 3.2, Pb = 45.9 ± 7.00 and V = 2.4 ± 1.6, expressed as the mean value of concentrations determined in the solutions during the last three years of the experiment, adequately represented the equilibrium in the solutions. The final molar ratios of the $Pb_{tot}$ to $Cl_{tot}$ in the solutions varied between 1.8 and 1.9, while the ratios of $Pb_{tot}$ to $V_{tot}$ fell in the range between 17 and 20. The proportions were neither typical for vanadinite (Pb:V;Cl = 5:3:1), nor for chervetite (Pb:V = 1:2), indicating dissolution in

which the properties of both involved phases simultaneously affect the composition of the solution.

**Table 1.** Selected parameters of experimental solutions: the raw and calculated data.

| Time | | Concentration μmol·dm$^{-3}$ $Pb_{tot.}$ | | | $V_{tot.}$ | | | $Cl_{tot.}$ | | | $[Pb]_{tot}/[V]_{tot}$ | $[Pb]_{tot}/[Cl]_{tot}$ | Log SI * Chervetite | Log IAP ** Vanadinite | Log IAP *** Vanadinite |
|---|---|---|---|---|---|---|---|---|---|---|---|---|---|---|---|
| weeks | 0.1 | 5.7 | ± | 0.4 | b.d. | ± | - | 8.3 | ± | 11.0 | - | 0.7 | - | - | - |
| | 0.7 | 18.5 | ± | 18.6 | b.d. | ± | - | 18.1 $_c$ | ± | 11.1 | - | 1.0 | - | - | - |
| | 2.0 | 19.6 | ± | 1.4 | b.d. | ± | - | 19.2 $_c$ | ± | 11.2 | - | 1.0 | - | - | - |
| | 4.6 | 24.0 | ± | 0.7 | b.d. | ± | - | 20.9 $_c$ | ± | 11.2 | - | 1.1 | - | - | - |
| | 7.7 | 26.7 | ± | 0.8 | b.d. | ± | - | 23.1 $_c$ | ± | 4.0 | - | 1.2 | - | - | - |
| | 13.4 | 27.5 | ± | 2.7 | 0.37 | ± | 0.04 | 14.9 | ± | 6.4 | 75 | 1.8 | −0.68 | −92.43 | −94.57 |
| | 18.9 | 28.5 | ± | 2.0 | 0.50 | ± | 0.04 | 20.2 $_c$ | ± | 5.2 | 57 | 1.4 | −0.56 | −92.28 | −94.05 |
| | 23.9 | 28.4 | ± | 0.7 | 0.46 | ± | 0.08 | 18.6 | ± | 5.6 | 62 | 1.5 | −0.59 | −92.32 | −94.17 |
| | 116 | 46.3 $_a$ | ± | 10.6 | 2.39 $_b$ | ± | 0.86 | 24.8 $_c$ | ± | 4.0 | 19 | 1.9 | 0.14 | −91.87 | −91.42 |
| | 132 | 45.6 $_a$ | ± | 3.0 | 2.62 $_b$ | ± | 2.84 | 23.4 $_c$ | ± | 4.0 | 17 | 1.9 | 0.16 | −91.91 | −91.39 |
| | 147 | 45.8 $_a$ | ± | 4.4 | 2.28 $_b$ | ± | 1.61 | 25.2 $_c$ | ± | 4.5 | 20 | 1.8 | 0.13 | −91.87 | −91.47 |

* logarithm of Saturation Index for Chervetite in the solution calculated with the use of the geochemical model PHREEQC (Phreeqc Interactive 3.5.0-14000) [64]; for undersaturated solution SI < 0, for saturated solution SI = 0, for supersaturated solution SI > 0. ** Ion Activity Product (IAP) for Vanadinite calculated with the use of PHREEQC [64]—assuming solution equilibrated with Chervetite. *** Ion Activity Product (IAP) for Vanadinite calculated with the use of PHREEQC [64]—neglecting the presence of Chervetite. $_{a, b, c}$ Values within a column followed by the same letters are statistically identical at 95% confidence level. Shaded table rows represent equilibrium.

## 4. Discussion

Thermodynamic modelling of incongruent dissolutions poses significant challenges. In this regard, few approaches for the apatite group have been proposed [71–74]. In this study, the geochemical speciation model PHREEQC (Phreeqc Interactive 3.5.0-14000) [64] was used to support the calculations of thermodynamic parameters. The MINTEQA2 [70] was chosen as the PHREEQC database containing, in our opinion, the most comprehensive dataset related to vanadium compounds. The database did not include referenced thermodynamic data for vanadinite, since, to date, no reliable report has been proposed in these terms; however, the equilibrium constant of chervetite dissolution reaction (1) was indicated there as $10^{-0.95}$.

$$PbVO_{3.5} + 3H^+ = Pb^{2+} + VO^{2+} + 1.5H_2O \quad (1)$$

The compositions of the experimental solutions were proceeded with the use of PHREEQC [64] to verify their possible saturation with chervetite. The results presented as the logarithm of chervetite saturation index (SI) are shown in Table 1. The log SI values indicated supersaturation with chervetite for the last three years of the vanadinite dissolution. Even though the log SI values only slightly exceeded 0, the experimental conditions were favorable for vanadates polymerization as indicated by the PHREEQC modeling [64] and the precipitation of chervetite occurred as confirmed by the SEM/EDS and XRD analysis. Hence, there were two possible approaches to further the thermodynamic modeling of vanadinite's solubility product, $K_{sp}$: (i) acknowledging the equilibrium with chervetite or (ii) neglecting the presence of a secondary phase as having little effect on the equilibrium [71–74]. Both approaches were exercised using PHREEQC [64].

If the dissolution reaction of vanadinite is written as in the Equation (2),

$$Pb_5(VO_4)_3Cl = 5Pb^{2+} + 3VO_4{}^{3-} + Cl^- \quad (2)$$

then the logarithm of the ion activity product (IAP) for the reaction (2) is given by:

$$\log IAP = 5\log\{Pb^{2+}\} + 3\log\{PO_4{}^{3-}\} + \log\{Cl^-\} \quad (3)$$

where {} denotes activities of the ions. At equilibrium, the Ion Activity Product (IAP) calculated for the dissolution reaction of a mineral is equal to its solubility product, $K_{sp}$. The activities of aqueous $Pb^{2+}$, $VO_4{}^{3-}$, and $Cl^-$ were calculated considering the two different approaches: (i) and (ii) mentioned above with the use of the geochemical speciation model PHREEQC [64]. All reactions were modeled as open to the air with $P_{CO2} = 10^{-3.5}$ atm, at pH = 3.5 and temperature = 25 °C. The experimental concentrations of $Pb_{tot}$, $V_{tot}$ and

$Cl_{tot}$ were used as the input data and the calculated log IAPs are listed in Table 1. For all equilibrated solutions, the obtained values were of similar magnitude; however, the IAP values that neglected the presence of chervetite were slightly higher. At equilibrium, the average log IAP for vanadinite calculated based on the approach (i) was: −91.89 ± 0.05, whereas the average log IAP value obtained using the alternative approach (ii) was: −91.43 ± 0.08 (uncertainties represented by the double standard deviation from three values calculated at equilibrium).

To validate the calculations made upon the "inverse modeling" based on the three-step empirical approach with the use of the geochemical speciation model PHREEQC [64] was applied. In the first step of the inverse approach, the MINTEQA2 [65] thermodynamic database available in the PHREEQC [64] package was modified by the amendment of the dissolution reaction for vanadinite (4):

$$Pb_5(VO_4)_3Cl = 5Pb^{2+} + 3VO_4^{3-} + Cl^-;\ \text{log\_k} = X \quad (4)$$

where "log_k" expresses solubility product of vanadinite (log $K_{sp,V,298}$). In the second step, the value of the vanadinite solubility product (log $K_{sp,V,298}$) expressed by $X$ in the Equation (4) was modified in the database with the use of experimentally determined IAP values calculated at equilibrium (Table 1): $X$ = -90.87, -90.91, -90.42, −90.39 and -90.47. The input file of a modeling assumed (Appendix C):

- The concentration of background electrolyte KNO3 = 0.05 M;
- Constant temperature (24 °C, 25 °C or 26 °C);
- Initial fixed pH = 3.5;
- Forced equilibrium of the solution with the vanadinite and chervetite.

In the third step, the output data of each modeling were compared with the results of the dissolution experiment, in terms of the solution parameters such as: pH, total Pb, Cl and V concentrations and saturation index of other potentially precipitated phases. The obtained set of selected data is presented in Table 2.

**Table 2.** Comparison of the selected solution parameters determined in dissolution experiments of vanadinite and via computing with geochemical model PHREEQC [64].

| Method of Obtaining the Data | | | Equilibrium Concentration Pb (μmol dm$^{-3}$) | V (μmol dm$^{-3}$) | Cl (μmol dm$^{-3}$) | Residual Phases * |
|---|---|---|---|---|---|---|
| Experimental | | | 45.9 ± 7.0 $_a$ | 2.4 ± 1.6 $_b$ | 24.4 ± 3.2 $_c$ | none |
| Geochemical modeling assuming: ** | Approach (ii) | Log $K_{sp,V}$ = −90.42 | 66.5 ± 8.4 | 0.9 ± 0.2 $_b$ | 32.8 ± 4.3 | none |
| | | Log $K_{sp,V}$ = −91.47 | 64.0 ± 8.0 | 0.9 ± 0.2 $_b$ | 31.5 ± 4.1 | none |
| | | Log $K_{sp,V}$ = −91.39 | 68.0 ± 7.7 | 0.9 ± 0.2 $_b$ | 33.5 ± 3.9 | none |
| | Approach (i) | Log $K_{sp,V}$ = −91.87 | 47.3 ± 7.0 $_a$ | 1.4 ± 0.2 $_b$ | 22.9 ± 3.6 $_c$ | none |
| | | Log $K_{sp,V}$ = −91.91 | 45.9 ± 6.7 $_a$ | 1.5 ± 0.3 $_b$ | 22.2 ± 3.5 $_c$ | none |

* Phases other than Vanadinite and Chervetite; ** Geochemical modeling with the use of PHREEQC [64], in which the MINTEQA2 [65] database was amended with particular values of the solubility product of Vanadinite (log $K_{sp,V}$) listed in the column 3. Approach (i): acknowledging presence of Chervetite. Approach (ii): neglecting presence of Chervetite; ± Double standard deviation of triplicates (experimental data) or of modeling at three different temperatures (modeling data); $_{a, b, c,}$ Values within a column followed by the same letters are statistically identical at 95% confidence level.

The PHREEQC [64] calculations with the assumed vanadinite solubility products log $K_{sp,V,298}$ equal −90.87 and 90.91 yielded solution parameters that were statistically identical (at 95% confidence level) with the empirical results provided by the dissolution experiment. This suggested that the calculations acknowledging the presence of chervetite were more adequate in this case. Thus, we recommend the value ($K_{sp,V,298} = 10^{-91.89 \pm 0.05}$) as the first empirically determined solubility product of vanadinite which can be used for further thermodynamic calculations, modeling and experimental approximations. The uncertainty (±0.05) corresponds to a double standard deviation of the IAP values calculated for equilibrium in this study. The presented approach involving "inverse geochemical modeling" is a universal method to validate the assumptions made during thermodynamic modeling. The method is simple and in case of a complex incongruent dissolution systems it may refine uncertainties or even act as the straightforward calculations without intricate raw data processing. The obtained value ($K_{sp,V,298} = 10^{-91.89 \pm 0.05}$) is notably lower than the value ($K_{sp,V,298} = 10^{-86}$) proposed by Gerke et al. [10], however, their data was just an approximation based on presumptions of water parameters in lead-containing pipes and did not consider incongruent nature of vanadinite dissolution, precipitation of chervetite or equilibrium evidence in the solution. Nevertheless, regarding the general tendency of Pb-apatites for extremely low solubility products and the relative value of vanadinite parameter when compared to other Cl-Pb-apatites e.g., mimetite $K_{sp,V,298} = 10^{-79.11 \pm 0.33}$ [36] and pyromorphite $K_{sp,V,298} = 10^{-79.60 \pm 0.33}$ [39], our results were self-consistent.

## 5. Conclusions

For the first time, the experimentally determined solubility product of vanadinite equal to $K_{sp,V}$ $10^{-91.89 \pm 0.05}$ is presented. Vanadinite is an exceptional mineral among Pb-apatite series; it dissolves incongruently, inducing precipitation of chervetite as the sole secondary phase. The incongruent mechanism of vanadinite's dissolution poses a challenge to the direct experimental determination of the solubility constant; however, a new calculation approach, along with the unique, long term experiments proposed here, made it possible to overcome this difficulty. The approach to modeling with a use of the presented inverse method is novel, universal and can be applied to other systems.

**Author Contributions:** Conceptualization, J.T., B.P. and M.M.; methodology, J.T.; formal analysis, J.T., B.P. and M.M.; investigation J.T., B.P., O.B., J.S. and M.M.; resources, J.T. and M.M.; data curation, J.T.; writing—original draft preparation, J.T.; writing—review and editing, J.T., B.P., O.B., J.S. and M.M.; visualization, J.T. and J.S.; supervision, J.T.; project administration, J.T.; funding acquisition, J.T. and M.M. All authors have read and agreed to the published version of the manuscript.

**Funding:** This research was funded by the AGH University of Science and Technology grant number 16.16.140.315.

**Institutional Review Board Statement:** Not applicable.

**Informed Consent Statement:** Not applicable.

**Acknowledgments:** We would like to thank Beata Ostachowicz and Gabriela Kozub-Budzyń from AGH University of Science and Technology for technical help in analysis. We thank three anonymous experts for their detailed reviews that helped us to improve the manuscript.

**Conflicts of Interest:** The authors declare no conflict of interest.

## Appendix A

**Table A1.** Powder X-ray diffraction peaks from synthetic $Pb_5(VO_4)_3Cl$ used in this study compared with data reported in the literature: Miller indices *h k l*, distance *d* between adjacent (*h k l*) planes and the peak intensity ratio *I/Io*.

| *h k l* | Vanadinite $Pb_5(VO_4)_3Cl$ | | | | | | Dissolution Residuum, This Study | | Chervetite $Pb_2V_2O_7$ | | | | *h k l* |
|---|---|---|---|---|---|---|---|---|---|---|---|---|---|
| | Dai and Hughes [66] | | Trotter and Barnes [67] | | Synthesis, This Study | | | | [70] | | [69] | | |
| | *d*-Spacing (Å) | *I/Io* | *d*-Spacing/ (Å) | *I/Io* | *d*-Spacing/ (Å) | *I/Io* | *d*-Spacing/ (Å) | *I/Io* | *d*-Spacing/ (Å) | *I/Io* | *d*-Spacing/ (Å) | *I/Io* | |
| 110 | 5.1587 | 7.83 | 5.1655 | 8.91 | 5.171 | 7 | 5.170 | 10 | | | | | |
| | | | | | | | 4.998 | 4 | 4.9545 | 6.98 | 4.9573 | 7.26 | $\bar{1}11$ |
| | | | | | | | 4.949 | 15 | 4.9422 | 57.75 | 4.9438 | 61.74 | 011 |
| 200 | 4.4676 | 24.21 | 4.4735 | 25.16 | 4.476 | 20 | 4.475 | 29 | | | | | |
| | | | | | | | 4.339 | 9 | 4.3337 | 37.88 | 4.3337 | 42.95 | 111 |
| 111 | 4.2202 | 32.9 | 4.2249 | 34.62 | 4.230 | 27 | 4.227 | 30 | | | | | |
| | | | | | | | 4.155 | 6 | 4.1469 | 4.71 | 4.1460 | 3.79 | 201 |
| 201 | 3.8159 | 4.89 | 3.8203 | 2.97 | 3.824 | 4 | 3.828 | 5 | | | | | |
| | | | | | | | 3.680 | 5 | 3.6770 | 1.66 | 3.6762 | 1.59 | 310 |
| 002 | 3.6689 | 7.66 | 3.6715 | 6.84 | 3.678 | 8 | | | | | | | |
| | | | | | | | 3.592 | 14 | 3.5886 | 60.57 | 3.5879 | 61.34 | 211 |
| | | | | | | | 3.450 | 22 | 3.4491 | 100 | 3.4487 | 100 | 120 |
| | | | | | | | 3.433 | 15 | 3.4312 | 66.96 | 3.4351 | 76.92 | $\bar{2}02$ |
| 102 | 3.3939 | 26.22 | 3.3966 | 26.95 | 3.390 | 38 | 3.403 | 14 | | | | | |
| 120, 210 | 3.3772 | 17.03, 18.84 | 3.3816 | 14.39, 19.26 | | | 3.381 | 29 | | | | | |
| | | | | | | | 3.273 | 4 | 3.2749 | 18.70 | 3.2761 | 18.90 | $\bar{4}01$ |
| | | | | | | | 3.217 | 29 | 3.2138 | 85.59 | 3.2130 | 83.30 | 400 |
| | | | | | | | 3.188 | 4 | 3.1815 | 15.91 | 3.1840 | 12.88 | $\bar{1}12$ |
| | | | | | | | 3.172 | 10 | 3.1743, 3.1710 | 1.48, 32.64 | 3.1748, 3.1713 | 2.11, 33.84 | $\bar{1}21$, 021 |
| 121, 211 | 3.0678 | 45,76, 54.24 | 3.0716 | 46.19, 53.81 | 3.073, 2.993 | 94, 100 | 3.073 | 100 | | | | | |
| 112 | 2.9899 | 95.04 | 2.9926 | 91.58 | | | 2.996 | 65 | | | | | |
| 300 | 2.9784 | 53.24 | 2.9823 | 55.19 | 2.841 | 1 | 2.982 | 28 | | | | | |
| | | | | | | | 2.934 | 6 | 2.9320 | 12.83 | 2.9314 | 11.63 | 410 |
| | | | | | | | 2.863 | 6 | 2.8607 | 30.45 | 2.8633 | 35.03 | $\bar{3}12$ |
| | | | | | | | 2.839 | 4 | 2.8419 | 13.05 | 2.8427 | 16.40 | 112 |
| 301 | 2.7597 | 1.45 | 2.7631 | 1.16 | 2.763 | 1 | | | | | | | |
| | | | | | | | 2.748 | 8 | 2.7475 | 28.12 | 2.7471 | 27.05 | 320 |
| | | | | | | | 2.724 | 7 | 2.7219 | 41.21 | 2.7221 | 41.71 | 202 |
| | | | | | | | 2.711 | 5 | 2.7100 | 27.44 | 2.7096 | 26.70 | 221 |
| 220 | 2.5793 | 2.89 | 2.5828 | 1.99 | 2.582 | 3 | 2.585 | 5 | | | | | |
| | | | | | | | 2.519 | 6 | 2.5213 | 23.04 | 2.5225 | 25.58 | $\bar{1}22$ |
| 122 | 2.4848 | 2.01 | 2.4873 | 1.96 | 2.489 | 3 | 2.493 | | | | | | |
| | | | | | | | 2.419 | 4 | 2.4198 | 3.64 | 2.4192 | 3.61 | 510 |
| | | | | | | | 2.351 | 4 | 2.3525 | 10.57 | 2.3538 | 11.55 | $\bar{3}22$ |
| 131 | 2.3479 | 1.27 | 2.3508 | 1.40 | 2.350 | 1 | | | | | | | |
| 302 | 2.3124 | 5.55 | 2.3149 | 4.43 | 2.316 | 6 | 2.316 | 6 | | | | | |
| | | | | | | | 2.276 | 5 | 2.2766, 2.2704 | 17.94, 2.40 | 2.2782, 2.2720 | 20.30, 2.96 | 003, $\bar{5}12$ |
| | | | | | | | 2.237 | 13 | 2.2376 | 23.01, 2.51 | 2.2394, 2.2373 | 1.62, 24.71 | $\bar{1}13$, 230 |
| 400 | 2.2338 | 5.48 | 2.2367 | 4.94 | 2.238 | 5 | | | | | | | |
| 113 | 2.2101 | 10.66 | 2.2119 | 9.69 | 2.214 | 9 | 2.215 | 7 | | | | | |
| | | | | | | | 2.184 | 4 | 2.1892, 2.1860 | 6.51, 12.57 | 2.1893, 2.1859 | 8.28, 12.40 | $\bar{2}31$, 131 |
| | | | | | | | 2.127 | 5 | 2.1259, 2.1258 | 2.07, 17.04 | 2.1262, 2.1252 | 1.12, 18.00 | $\bar{6}11$, 421 |
| 222 | 2.1101 | 35.78 | 2.1124 | 34.74 | 2.114 | 33 | 2.114 | 29 | 2.1153 | 10.67 | 2.1145 | 11.02 | 511 |
| | | | | | | | 2.090 | 8 | 2.0918 | 6.17 | 2.0930 | 7.02 | $\bar{6}02$ |
| | | | | | | | 2.068 | 5 | 2.0687 | 2.61 | 2.0684 | 3.73 | 231 |
| 132, 312 | 2.0536 | 3.93, 12.51 | 2.0559 | 5.09, 12.68 | 2.055 | 18 | 2.056 | 15 | | | | | |
| | | | | | | | 2.006 | 4 | 2.0078 | 21.67 | 2.0090 | 23.93 | $\bar{6}12$ |
| 123, 213 | 1.9810 | 17.15, 11.10 | 1.9828 | 15.11, 10.38 | 1.982 | 28 | 1.984 | 13 | 1.9810 | 5.89 | 1.9815 | 8.14 | $\bar{1}32$ |
| | | | | | | | 1.977 | 13 | 1.9774 | 15.87 | 1.9772 | 17.79 | 322 |
| 140, 410 | 1.9498 | 8.28, 16.55 | 1.9524 | 7.87, 14.76 | 1.952 | 21 | 1.952 | 20 | | | | | |
| 402 | 1.9080 | 28.52 | 1.9102 | 28.36 | 1.911 | 25 | 1.911 | 21 | | | | | |
| | | | | | | | 1.891 | 4 | 1.8906 | 6.31 | 1.8907 | 6.84 | $\bar{6}21$ |
| | | | | | | | 1.838 | 11 | 1.8388 | 2.54 | 1.8393 | 2.13 | 123 |
| 004 | 1.8345 | 12.99 | 1.8357 | 12.81 | 1.838 | 12 | | | | | | | |
| 322 | 1.7895 | 1.69 | 1.7916 | 1.20 | 1.791 | 2 | 1.791 | 4 | | | | | |
| | | | | | | | 1.732 | 5 | 1.7337 | 1.36 | 1.7340 | 1.52 | 223 |

## Appendix B

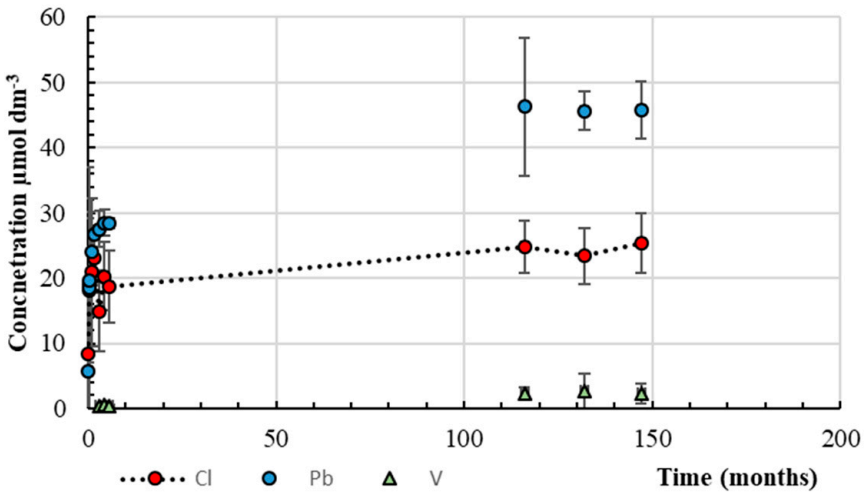


**Figure A1.** The evolution of $Pb_{tot}$, $Cl_{tot}$ and $V_{tot}$ concentrations in the experimental solutions with time.

## Appendix C

Exemplary input data for PHREEQC simulation used for "Inverse modeling".

```
SOLUTION 1
    temp      25
    pe        4
    redox     pe
    units     mmol/kgw
    density   1
    -water    1 # kg
     K        50
     N(5) 50
PHASES
  pH_Fix
   H+ = H+
    log_K = 0.0
Vanadinite
        Pb5(VO4)3Cl = 5Pb+2 + 3VO4-3 + Cl−
        log_k     −91.87

EQUILIBRIUM_PHASES 1
    CO2(g)      −3.5      1.0
chervetite   0.0
    Vanadinite   0.0
    pH_Fix      −3.5     HNO3        10.0
      -force_equality
END
```

## References


1. Crans, D.C.; Smee, J.J.; Gaidamauskas, E.; Yang, L. The chemistry and biochemistry of vanadium and the biological activities exerted by vanadium compounds. *Chem. Rev.* **2004**, *104*, 849–902. [CrossRef] [PubMed]
2. Hubregtse, T.; Neeleman, E.; Maschmeyer, T.; Sheldon, R.A.; Hanefeld, U.; Arends, I.W.C.E. The first enantioselective synthesis of the amavadin ligand and its complexation to vanadium. *J. Inorg. Biochem.* **2005**, *99*, 1264–1267. [CrossRef] [PubMed]
3. Kraepiel, A.M.L.; Bellenger, J.P.; Wichard, T.; Morel, F.M.M. Multiple roles of siderophores in free-living nitrogen-fixing bacteria. *Biometals* **2009**, *22*, 573–581. [CrossRef] [PubMed]
4. Renirie, R.; Charnock, J.M.; Garner, C.D.; Wever, R. Vanadium K-edge XAS studies on the native and peroxo-forms of vanadium chloroperoxidase from Curvularia inaequalis. *J. Inorg. Biochem.* **2010**, *104*, 657–664. [CrossRef] [PubMed]
5. Ceci, A.; Kierans, M.; Hillier, S.; Persiani, A.M.; Gadd, G.M. Fungal bioweathering of mimetite and a general geomycological model for lead apatite mineral biotransformations. *Appl. Environ. Microbiol.* **2015**, *81*, 4955–4964. [CrossRef] [PubMed]

6. Ramasarma, T.; Venkataraman, B.V. A perspective of smooth muscle contractility through actions of vanadium compounds. *Indian J. Physiol. Pharmacol.* **1999**, *43*, 277–295.
7. Ceci, A.; Rhee, Y.J.; Kierans, M.; Hillier, S.; Pendlowski, H.; Gray, N.; Persiani, A.M.; Gadd, G.M. Transformation of vanadinite [Pb 5 (VO 4) 3 Cl] by fungi: Fungal biotransformation of vanadinite. *Environ. Microbiol.* **2015**, *17*, 2018–2034. [CrossRef]
8. Ertl, A.; Rakovan, J.; Hughes, J.M.; Bernhardt, H.-J.; Rossman, G.R. Vanadium-rich Muscovite from Austria: Crystal structure, chemical analysis, and spectroscopic investigations. *Can. Miner.* **2019**, *57*, 383–389. [CrossRef]
9. Stoppa, F.; Schiazza, M.; Rosatelli, G.; Castorina, F.; Sharygin, V.V.; Ambrosio, F.A.; Vicentini, N. Italian carbonatite system: From mantle to ore-deposit. *Ore Geol. Rev.* **2019**, *114*, 103041. [CrossRef]
10. Gerke, T.L.; Scheckel, K.G.; Schock, M.R. Identification and distribution of vanadinite (Pb5($V^{5+}$O4)3Cl) in lead pipe corrosion by-products. *Environ. Sci. Technol.* **2009**, *43*, 4412–4418. [CrossRef]
11. Gerke, T.L.; Scheckel, K.G.; Maynard, J.B. Speciation and distribution of vanadium in drinking water iron pipe corrosion by-products. *Sci. Total. Environ.* **2010**, *408*, 5845–5853. [CrossRef] [PubMed]
12. Markl, G.; Marks, M.A.W.; Holzäpfel, J.; Wenzel, T. Major, minor, and trace element composition of pyromorphite-group minerals as recorder of supergene weathering processes from the Schwarzwald mining district, SW Germany. *Am. Miner.* **2014**, *99*, 1133–1146. [CrossRef]
13. Song, H.; Liu, J.; Cheng, H. Structural and spectroscopic study of arsenate and vanadate incorporation into apatite group: Implications for semi-quantitative estimation of As and V contents in apatite. *Spectrochim. Acta Part A Mol. Biomol. Spectrosc.* **2018**, *188*, 488–494. [CrossRef] [PubMed]
14. Solecka, U.; Bajda, T.; Topolska, J.; Zelek-Pogudz, S.; Manecki, M. Raman and fourier transform infrared spectroscopic study of pyromorphite-vanadinite solid solutions. *Spectrochim. Acta Part A Mol. Biomol. Spectrosc.* **2018**, *190*, 96–103. [CrossRef] [PubMed]
15. Hu, Z.; Petoukhov, S.V.; He, M. Advances in artificial systems for medicine and education II. In *Advances in Intelligent Systems and Computing*; Shakhovska, N., Ed.; Springer: Berlin/Heidelberg, Germany, 2020.
16. Pasero, M.; Kampf, A.R.; Ferraris, C.; Pekov, I.V.; Rakovan, J.; White, T.J. Nomenclature of the apatite supergroup minerals. *Eur. J. Miner.* **2010**, *22*, 163–179. [CrossRef]
17. Cockbain, A.G. The crystal chemistry of the apatites. *Miner. Mag. J. Miner. Soc.* **1968**, *36*, 654–660. [CrossRef]
18. White, T.J.; Zhili, D. Structural derivation and crystal chemistry of apatites. *Acta Crystallogr. Sect. B Struct. Sci.* **2003**, *59*, 1–16. [CrossRef]
19. Frost, R.L.; Crane, M.; Williams, P.A.; Kloprogge, J.T. Isomorphic substitution in vanadinite [Pb5(VO4)3Cl]?—A raman spectroscopic study. *J. Raman Spectrosc.* **2003**, *34*, 214–220. [CrossRef]
20. Baikie, T.; Mercier, P.H.J.; Elcombe, M.M.; Kim, J.Y.; Le Page, Y.; Mitchell, L.D.; White, T.J.; Whitfield, P.S. Triclinic apatites. *Acta Crystallogr. Sect. B Struct. Sci.* **2007**, *63*, 251–256. [CrossRef]
21. Baikie, T.; Ferraris, C.; Klooster, W.T.; Madhavi, S.; Pramana, S.S.; Pring, A.; Schmidt, G.; White, T.J. Crystal chemistry of mimetite, Pb10(AsO4)6Cl1.48O0.26, and finnemanite, Pb10(AsO3)6Cl2. *Acta Crystallogr. Sect. B Struct. Sci.* **2008**, *64*, 34–41. [CrossRef]
22. Bajda, T.; Mozgawa, W.; Manecki, M.; Flis, J. Vibrational spectroscopic study of mimetite–pyromorphite solid solutions. *Polyhedron* **2011**, *30*, 2479–2485. [CrossRef]
23. Baikie, T.; Schreyer, M.; Wei, F.; Herrin, J.S.; Ferraris, C.; Brink, F.; Topolska, J.; Piltz, R.O.; Price, J.; White, T.J. The influence of stereochemically active lone-pair electrons on crystal symmetry and twist angles in lead apatite-2 H type structures. *Miner. Mag.* **2014**, *78*, 325–345. [CrossRef]
24. Sordyl, J.; Puzio, B.; Manecki, M.; Borkiewicz, O.J.; Topolska, J.; Zelek-Pogudz, S. Structural Assessment of Fluorine, Chlorine, bromine, iodine, and hydroxide substitutions in lead arsenate apatites (mimetites)–Pb5(AsO4)3X. *Minerals* **2020**, *10*, 494. [CrossRef]
25. Ewing, R.C.; Wang, L. Phosphates as nuclear waste forms. *Rev. Miner. Geochem.* **2002**, *48*, 673–699. [CrossRef]
26. Dong, Z.; White, T.J.; Wei, B.; Laursen, K. Model apatite systems for the stabilization of toxic metals: I, calcium lead vanadate. *J. Am. Ceram. Soc.* **2002**, *85*, 2515–2522. [CrossRef]
27. Kim, J.Y.; Dong, Z.; White, T.J. Model apatite systems for the stabilization of toxic metals: II, cation and metalloid substitutions in chlorapatites. *J. Am. Ceram. Soc.* **2005**, *88*, 1253–1260. [CrossRef]
28. Madhavi, S.; Ferraris, C.; White, T.J. Cadmium and lead ion capture with three dimensionally ordered macroporous hydroxyapatite. *Environ. Sci. Technol.* **2006**, *40*, 7054–7059. [CrossRef]
29. Oelkers, E.H.; Montel, J.-M. Phosphates and nuclear waste storage. *Elements* **2008**, *4*, 113–116. [CrossRef]
30. Oelkers, E.H.; Valsami-Jones, E. Phosphate mineral reactivity and global sustainability. *Elements* **2008**, *4*, 83–87. [CrossRef]
31. Majzlan, J. Thermodynamic stabilization of hydrous ferric oxide by adsorption of phosphate and arsenate. *Environ. Sci. Technol.* **2011**, *45*, 4726–4732. [CrossRef]
32. Rakovan, J.F.; Pasteris, J.D. A Technological gem: Materials, medical, and environmental mineralogy of Apatite. *Elements* **2015**, *11*, 195–200. [CrossRef]
33. Bhattacharjee, A.; Fang, Y.N.; Hooper, T.J.; Kelly, N.L.; Gupta, D.; Balani, K.; Manna, I.; Baikie, T.; Bishop, P.T.; White, T.J.; et al. Crystal Chemistry and Antibacterial Properties of Cupriferous Hydroxyapatite. *Materials* **2019**, *12*, 1814. [CrossRef]
34. Kanagawa, S.; Dong, Z.; Baikie, T.; White, T.; Takeshita, K. Synthesis and characterization of apatite wasteforms using simulated radioactive liquid waste. *Chem. Lett.* **2019**, *48*, 881–884. [CrossRef]

35. Topolska, J.; Latowski, D.; Kaschabek, S.; Manecki, M.; Merkel, B.J.; Rakovan, J. Pb remobilization by bacterially mediated dissolution of pyromorphite $Pb_5(PO_4)_3Cl$ in presence of phosphate solubilizing Pseudomonas putida. *Environ. Sci. Poll. Res.* **2014**, *21*, 1079–1089. [CrossRef] [PubMed]
36. Bajda, T. Solubility of mimetite Pb5(AsO4)3Cl at 5–55 °C. *Environ. Chem.* **2010**, *7*, 268–278. [CrossRef]
37. Flis, J.; Manecki, M.; Bajda, T. Solubility of pyromorphite Pb5(PO4)3Cl–mimetite Pb5(AsO4)3Cl solid solution series. *Geochim. Cosmochim. Acta* **2011**, *75*, 1858–1868. [CrossRef]
38. Xie, Y.; Giammar, D.E. Effects of flow and water chemistry on lead release rates from pipe scales. *Water Res.* **2011**, *45*, 6525–6534. [CrossRef]
39. Topolska, J.; Manecki, M.; Bajda, T.; Borkiewicz, O.; Budzewski, P. Solubility of pyromorphite Pb5(PO4)3Cl at 5–65°C and its experimentally determined thermodynamic parameters. *J. Chem. Thermodyn.* **2016**, *98*, 282–287. [CrossRef]
40. Ma, Q.Y.; Traina, S.J.; Logan, T.J.; Ryan, J.A. In situ lead immobilization by apatite. *Environ. Sci. Technol.* **1993**, *27*, 1803–1810. [CrossRef]
41. Manecki, M.; Maurice, P.A.; Traina, S.J. Uptake of aqueous Pb by Cl−, F−and OH−apatites: Mineralogic evidence for nucleation mechanisms. *Am. Miner.* **2000**, *85*, 932–942.
42. Miretzky, P.; Fernandez-Cirelli, A. Phosphates for Pb immobilization in soils: A review. *Environ. Chem. Lett.* **2008**, *6*, 121–133. [CrossRef]
43. Park, J.H.; Bolan, N.; Megharaj, M.; Naidu, R. Concomitant rock phosphate dissolution and lead immobilization by phosphate solubilizing bacteria (Enterobacter sp.). *J. Environ. Manag.* **2011**, *92*, 1115–1120. [CrossRef] [PubMed]
44. Imtiaz, M.; Rizwan, M.S.; Xiong, S.; Li, H.; Ashraf, M.; Shahzad, S.M.; Shahzad, M.; Rizwan, M.; Tu, S. Vanadium, recent advancements and research prospects: A review. *Environ. Int.* **2015**, *80*, 79–88. [CrossRef] [PubMed]
45. Ray, R.; Dutta, B.; Mandal, S.K.; González, A.G.; Pokrovsky, O.S.; Jana, T.K. Bioaccumulation of vanadium (V), niobium (Nb) and tantalum (Ta) in diverse mangroves of the Indian Sundarbans. *Plant. Soil* **2020**, *448*, 553–564. [CrossRef]
46. World Health Organisation. Vanadium. In *Air Quality Guidelines*, 2nd ed.; World Health Organization, Regional Office for Europe, Ed.; World Health Organization: Copenhagen, Denmark, 2000; pp. 170–172.
47. Agency for Toxic Substances and Disease Registry; Environmental Protection Agency. *Toxicological Profile for Vanadium*; US Department of Health and Human Services; Public Health Service: Atlanta, GA, USA, 2012.
48. Gatta, G.D.; Lee, Y.; Kao, C.-C. Elastic behavior of vanadinite, Pb10(VO4)6Cl2, a microporous non-zeolitic mineral. *Phys. Chem. Miner.* **2008**, *36*, 311–317. [CrossRef]
49. Suetsugu, Y. Synthesis of lead vanadate iodoapatite utilizing dry mechanochemical process. *J. Nucl. Mater.* **2014**, *454*, 223–229. [CrossRef]
50. Lei, P.; Yao, T.; Gong, B.; Zhu, W.; Ran, G.; Lian, J. Spark plasma sintering-densified vanadinite apatite-based chlorine waste forms with high thermal stability and chlorine confinement. *J. Nucl. Mater.* **2020**, *528*, 151857. [CrossRef]
51. Petit, S.; Thomas, C.; Millot, Y.; Krafft, J.; Laberty-Robert, C.; Costentin, G. Activation of C−H bond of propane by strong basic sites generated by bulk proton conduction on v-modified hydroxyapatites for the formation of propene. *Chemcatchem* **2020**, *12*, 2506–2521. [CrossRef]
52. Knyazev, A.V.; Bulanov, E.N.; Smirnova, N.N.; Kuznetsova, N.Y.; Letyanina, I.A.; Pryamova, E.D. Thermodynamic properties of pentalead tris(vanadate) chloride. *Thermochim. Acta* **2011**, *515*, 79–83. [CrossRef]
53. Schindler, M.; Hawthorne, F.C.; Baur, W.H. A crystal-chemical approach to the composition and occurrence of vanadium minerals. *Can. Miner.* **2000**, *38*, 1443–1456. [CrossRef]
54. Evans, J.H.T.; Garrels, R.M. Thermodynamic equilibria of vanadium in aqueous systems as applied to the interpretation of the Colorado Plateau ore deposits. *Geochim. Cosmochim. Acta* **1958**, *15*, 131–149. [CrossRef]
55. Topolska, J.; Bajda, T.; Puzio, B.; Manecki, M.; Kozub-Budzyń, G.K.-B. Time constraints on experimental studies of lead apatites. *Geol. Q.* **2019**, *63*, 721–728. [CrossRef]
56. Breit, G.N.; Wanty, R.B. Vanadium accumulation in carbonaceous rocks: A review of geochemical controls during deposition and diagenesis. *Chem. Geol.* **1991**, *91*, 83–97. [CrossRef]
57. Lu, X.; Johnson, W.D.; Hook, J. Reaction of vanadate with aquatic humic substances: An ESR and 51V NMR study. Environ. *Scien. Technol.* **1998**, *32*, 2257–2263. [CrossRef]
58. Bruyère, V.I.; Rodenas, L.A.G.; Morando, P.J.; Blesa, M.A. Reduction of vanadium (V) by oxalic acid in aqueous acid solutions. *J. Chem. Soc. Dalton Trans.* **2001**, *24*, 3593–3597. [CrossRef]
59. Gustafsson, J.P. Vanadium geochemistry in the biogeosphere–speciation, solid-solution interactions, and ecotoxicity. *App. Geochem.* **2019**, *102*, 1–25. [CrossRef]
60. Cornelis, G.; Van Gerven, T.; Snellings, R.; Verbinnen, B.; Elsen, J.; Vandecasteele, C. Stability of pyrochlores in alkaline matrices: Solubility of calcium antimonate. *Appl. Geochem.* **2011**, *26*, 809–817. [CrossRef]
61. Merchán, D.; Auqué, L.F.; Acero, P.; Gimeno, M.J.; Causape, J. Geochemical processes controlling water salinization in an irrigated basin in Spain: Identification of natural and anthropogenic influence. *Sci. Total. Environ.* **2015**, *502*, 330–343. [CrossRef]
62. Dangla, P.; Thiéry, M.; Morandeau, A. Thermodynamic of incongruent solubility of C–S–H. *Adv. Cem. Res.* **2015**, *27*, 601–609. [CrossRef]
63. Sahai, N.; Schoonen, M.A. Accuracy of thermodynamic databases for hydroxyapatite dissolution Constant. *Astrobiology* **2020**, *20*, 157–160. [CrossRef]

64. Parkhurst, D. User's guide to PHREEQC, a computer program for speciation, reaction-path, advective-transport, and inverse geochemical calculations. *USA Geol. Surv. Rep.* **1995**, 95–4227. [CrossRef]
65. Allison, J.D.; Brown, D.S.; Novo-Gradac, K.J. *MINTEQA2/PRODEFA2, A Geochemical Assessment Model for Environmental Systems: Version 3.0 User's Manual*; Environmental Research Laboratory; USA Environmental Protection Agency: Athens, GA, USA, 1991; p. 92.
66. Dai, Y.S.; Hughes, J.M. Crystal-structure refinements of vanadinite and pyromorphite. *Can. Min.* **1989**, *27*, 189–192.
67. Trotter, J.; Barnes, W.H. The structure of vanadinite. *Can. Min.* **1958**, *6*, 161–173.
68. Puzio, B.; Manecki, M.; Kwaśniak-Kominek, M. Transition from endothermic to exothermic dissolution of Hydroxyapatite Ca5(PO4)3OH–Johnbaumite Ca5(AsO4)3OH solid solution series at temperatures ranging from 5 to 65 °C. *Minerals* **2018**, *8*, 281. [CrossRef]
69. Kawahara, A. La structure cristalline de la chervétite. *Bull. Soc. Française Minéral. Cristallogr.* **1967**, *90*, 279–284. [CrossRef]
70. Shannon, R.D.; Calvo, C. Refinement of the crystal structure of synthetic chervetite, $Pb_2V_2O_7$. *Can. J. Chem.* **1973**, *51*, 70–76. [CrossRef]
71. Zhu, Y.; Zhang, X.; Chen, Y.; Xie, Q.; Lan, J.; Qian, M.; He, N. A comparative study on the dissolution and solubility of hydroxylapatite and fluorapatite at 25 °C and 45 °C. *Chem. Geol.* **2009**, *268*, 89–96. [CrossRef]
72. Liu, H.-L.; Zhu, Y.; Yu, H.-X. Solubility and stability of lead arsenates at 25 °C. *J. Environ. Sci. Health Part A* **2009**, *44*, 1465–1475. [CrossRef]
73. Zhang, X.; Zhu, Y.; Zeng, H.; Wang, D.; Liu, J.; Liu, H.; Qian, M.; Xu, L. Dissolution and solubility of the arsenate–phosphate hy-droxylapatite solid solution [Ca5(PxAs1–xO4)3(OH)] at 25 °C. *Environ. Chem.* **2011**, *8*, 133–145.
74. Zhu, Y.; Huang, B.; Zhu, Z.; Liu, H.; Huang, Y.; Zhao, X.; Liang, M. Characterization, dissolution and solubility of the hydroxypyromorphite–hydroxyapatite solid solution [(PbxCa1−x)5(PO4)3OH] at 25 °C and pH 2–9. *Geochem. Trans.* **2016**, *17*, 2–9. [CrossRef]